

High-temperature Thermoelectric Properties of Late Rare Earth-doped $\text{Ca}_3\text{Co}_2\text{O}_6$

Ngo Van Nong^{1,*} and Michitaka Ohtaki^{1,2}

¹Interdisciplinary Graduate School of Engineering Sciences, Kyushu University, Fukuoka, 816-8580, Japan
E-mail: nvnong@mm.kyushu-u.ac.jp

²CREST, Japan Science and Technology Agency, Kawaguchi, Saitama, 332-0012

Thermoelectric properties such as resistivity (ρ), Seebeck coefficient (S) and thermal conductivity (κ) of polycrystalline samples of late rare earth-doped $(\text{Ca}_{1-x}\text{Ln}_x)_3\text{Co}_2\text{O}_6$ with $\text{Ln} = \text{Ho}, \text{Dy}, \text{Tb}$ at $x = 0 - 0.05$ are investigated in the temperature range from room temperature to 1300 K. The Seebeck coefficient at temperatures higher than 500 K increases with increasing Ho concentration. The thermal conductivity of the samples decreases with increasing temperature, particularly at the high Ho concentrations. High temperature thermoelectric figure-of-merit (Z) of the samples is thereby improved by the rare-earth substitution, particularly those of Ho^{3+} for Ca^{2+} . The magnetic properties of the samples are also investigated and discussed.

Key words: one-dimensional structure, seebeck coefficient, electrical resistivity, thermal conductivity, figure-of-merit

1. INTRODUCTION

Thermoelectric devices have attracted much interest in terms of their potential application to clean energy-conversion systems. The conversion efficiency of a thermoelectric material is evaluated by the figure-of-merit $Z = S^2/\rho\kappa$, where S is the Seebeck coefficient, ρ is the electrical resistivity, and κ is the thermal conductivity. Oxides have thus been regarded as unsuitable for thermoelectric applications because of their high electrical resistivity resulting from poor mobility. However, the recent discovery of large thermopower coexisting with low electrical resistivity in Na_xCoO_2 and $\text{Ca}_3\text{Co}_4\text{O}_9$ has opened the way to the exploration of oxide thermoelectric materials [1-4]. The single crystal of these cobalt oxides exhibits good thermoelectric performance ($ZT > 1$ at 1000 K) [3], being competitive with conventional degenerate semiconductors such as Bi_2Te_3 , PbTe . However, since these cobalt oxides decompose at around 1100 K, materials of greater stability are required for power generation from waste heat in higher temperature regions, such as 627–1773 K in the steel industry and 473–1223 K in the ceramic industry.

Recently, $\text{Ca}_3\text{Co}_2\text{O}_6$ has intensively studied because of its interesting thermoelectric and magnetic properties [5-11]. This compound, which is stable in air up to 1300 K, has one-dimensional structure with the Co-O chains consisting of alternating face-sharing octahedra (containing Co1) and trigonal prisms (with Co2) along the hexagonal c-axis [5]. Recent researches on rare-earth containing cobalt perovskites, $(\text{Ca}, \text{R})\text{CoO}_3$ ($\text{R} = \text{Gd}, \text{Tb}, \text{Dy}, \text{Ho} \dots$), revealed that the figure-of-merit is enhanced and showed the largest value for the Ho substitution [12].

In this report, we focus on the high-temperature thermoelectric and magnetic properties of the Ho-doped polycrystalline samples denoted as $(\text{Ca}_{1-x}\text{Ho}_x)_3\text{Co}_2\text{O}_6$, in which the heavier Ho^{3+} ion substitutes for Ca^{2+} .

2. EXPERIMENTAL PROCEDURES

$(\text{Ca}_{1-x}\text{Ho}_x)_3\text{Co}_2\text{O}_6$ samples with $x = 0, 0.01, 0.03$ and 0.05 were synthesized by solid-state reaction starting from CaCO_3 (99.99%), Co_3O_4 (99.95%) and Ho_2O_3 (99.9%). These powders were mixed by rocking mill for 6h and in an agate mortar with ethanol. The mixtures were pressed into pellets and calcined in air at 1223 K for 24 h. The calcined samples were ground into powders and sintered at 1273 K in air for 48 h. The sintered samples were re-ground, pelletized and re-sintered under the same conditions for 48 h.

X-ray powder diffraction patterns were recorded on a diffractometer using CuK_α radiation. The electrical resistivity was measured by the direct-current four-probe method from 300 K to 1300 K. The thermal conductivity of the samples was measured from 300 K to 1100 K by laser flash method. The magnetic susceptibility and magnetization curves were measured by a SQUID magnetometer with the fields up to 5 T.

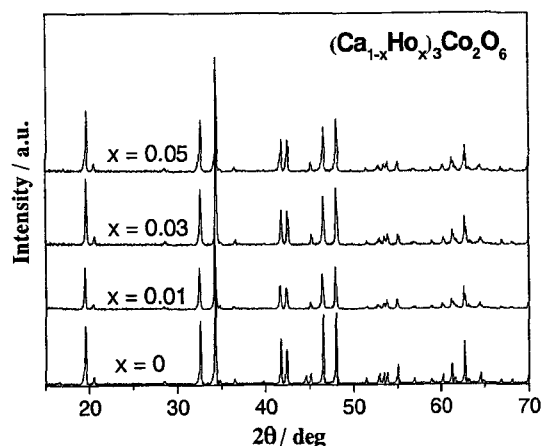


Fig.1 Powder X-ray diffraction patterns of the samples at room temperature.

3. RESULTS AND DISCUSSION

3.1 Thermoelectric properties

X-ray diffraction patterns of $(\text{Ca}_{1-x}\text{Ho}_x)_3\text{Co}_2\text{O}_6$ samples with $x = 0, 0.01, 0.03$ and 0.05 are shown in Fig. 1. These results and thermal analyses showed that they contain no impurity phases and are stable up to 1300 K.

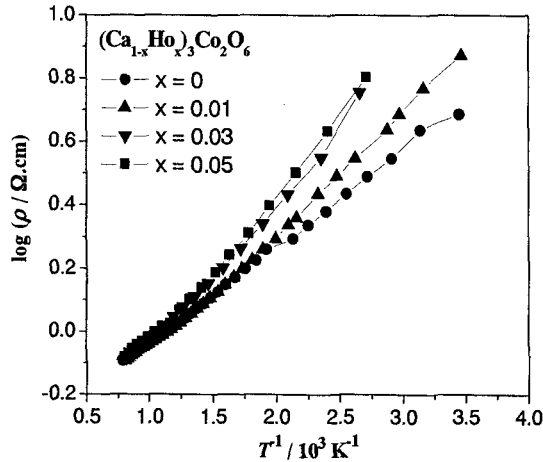


Fig.2 Temperature dependence of the electrical resistivity of the samples.

Fig. 2 shows the temperature dependence of the electrical resistivity for the samples. The ρ value decreases rapidly with increasing temperatures for all the samples in a temperature range of 300 to 1073 K. The relationship between $\log\rho$ and T^{-1} is linear in the lower temperature region, indicating a localized character of the carriers in the Co_2O_6 chains. It is reported that the transport character of $\text{Ca}_3\text{Co}_2\text{O}_6$ is consistent with one-dimensional structure, with the metal-metal intrachain distance (2.595 \AA) much shorter compared to the interchain separation (5.24 \AA) [11]. It is clear that the ρ values of the Ho-doped samples increased with increasing Ho concentration, particularly in the low temperature range. However, it should be noted that the resistivity of the samples converged with increasing temperature and the value became almost the same at about $1000 \text{ }^\circ\text{C}$. The increased resistivity can be explained by a decrease in the hole concentration due to the substitution of Ho^{3+} for Ca^{2+} ions.

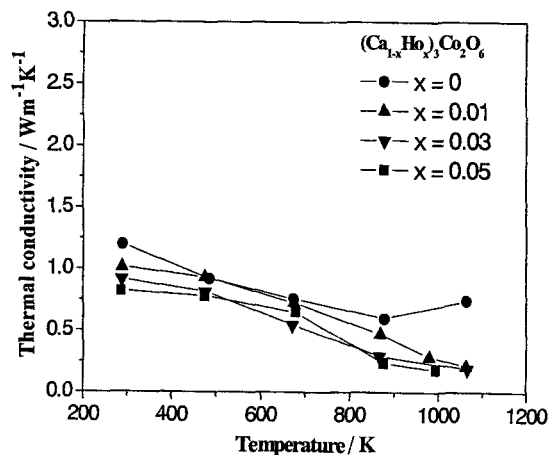


Fig.3 Thermal conductivity as a function of temperature of the samples.

Temperature dependence of the thermal conductivity for the samples is shown in Fig. 3. The total κ value of the Ho-doped samples decreased with increasing temperature and became remarkably low at the temperatures higher than 700 K. The contribution of the electronic component κ_{elec} to the sum total κ_{total} for the $\text{Ca}_3\text{Co}_2\text{O}_6$ sample estimated by using the Wiedemann-Franz relation is very small [11]. It indicates that the major contribution to the κ_{total} is the phonon term κ_{ph} . The decrease in the thermal conductivity is, therefore, attributed to the reduction of lattice component due to incorporation of heavier Ho^{3+} ion compared to Ca^{2+} ion.

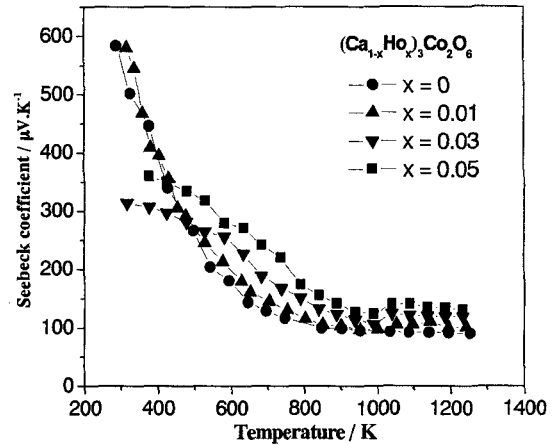


Fig.4. Temperature dependence of the Seebeck coefficient of the samples measured upon heating.

Fig. 4 shows the Seebeck coefficient as a function of temperature for the samples upon heating from 300 K to 1300 K. The Seebeck coefficients showed a positive value in the measured temperature range, indicating that the major conduction carriers are holes. Whereas the Seebeck coefficient of the $\text{Ca}_3\text{Co}_2\text{O}_6$ and the Ho-doped sample with $x = 0.01$ decreased rapidly with increasing temperature, S of the other samples decreases gradually to the S values higher than those of none-doped sample ($> 98 \mu\text{V.K}^{-1}$). It can also be seen clearly that the Seebeck coefficients increased with increasing Ho concentration at the temperatures higher than 500 K.

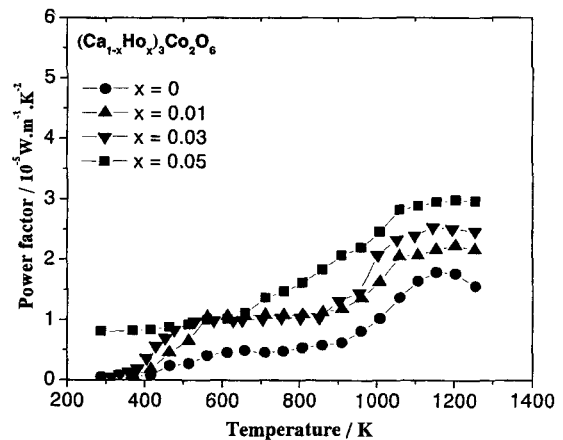


Fig.5 The temperature dependence of the power factor for the samples.

These results appear to be consistent with the decreases in the carrier concentrations. As discussed before,

however, the electrical resistivity of the samples was almost the same at about 1000 °C. These results suggest that there would be an enhancement of thermopower at high temperature.

Accordingly, the power factor derived from the electrical resistivity and Seebeck coefficient data showed a marked increase at high temperatures with increasing Ho concentration. Fig. 5 is the power factor as a function of temperature for the samples. At about 1058 K, the values of power factor are 1.37×10^{-5} , 2.05×10^{-5} , 2.39×10^{-5} and $2.82 \times 10^{-5} \text{ W.m}^{-1}.\text{K}^{-2}$ for the samples with $x = 0, 0.01, 0.03$ and 0.05 , respectively.

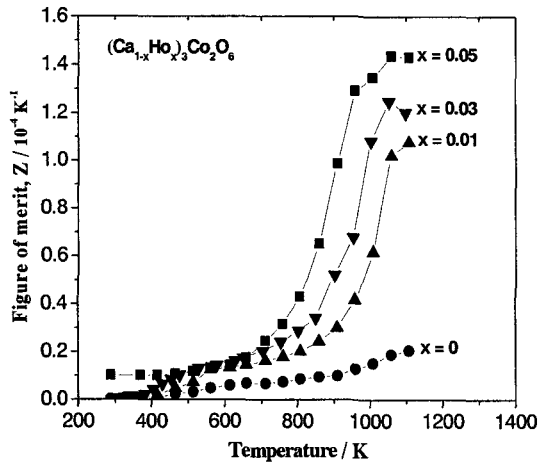


Fig.6 The figure-of-merit versus temperature of the samples

Finally, we calculated the thermoelectric figure-of-merit for the samples. Fig. 6 shows the temperature dependence of figure-of-merit, Z . The value of Z increased with increasing temperature and shows its maximum, 0.2×10^{-4} , 1.0×10^{-4} , 1.3×10^{-4} and $1.4 \times 10^{-4} \text{ K}^{-1}$ for the samples with $x = 0, 0.01, 0.03$ and 0.05 , respectively, at 1058 K. As a result of combining the decrease in the thermal conductivity and the increase in the power factor, the figure-of-merit was significantly enhanced at high temperature for the Ho-doped samples.

3.2 Magnetic properties

The temperature dependence of the magnetic susceptibility and inverse susceptibility of the samples are shown in Fig. 7. An anti-ferromagnetic (AF) peak can be observed at about $T_{C2} \sim 10 \text{ K}$ for the samples. This AF peak grew up with increasing Ho concentration, indicating the increase in the AF interaction between Co-O chains.

The inverse magnetic susceptibility showed clearly a paramagnetic behavior at temperatures higher than 80 K. The plots are linear and well follow the Curie-Weiss law. By using the Curie-Weiss equation, the effective magnetic moment (μ_{eff}) was calculated from magnetic susceptibility data. The obtained results are listed in the table I.

$$\chi = \frac{C}{T + \theta_p}$$

Table I: The effective magnetic moment (μ_{eff}) of the samples.

$(\text{Ca}_{1-x}\text{Ho}_x)_3\text{Co}_2\text{O}_6$	$\mu_{\text{eff}} (\mu_B)$
$x = 0$	5.03
$x = 0.01$	5.37
$x = 0.03$	5.78
$x = 0.05$	6.03

It is clear that the effective magnetic moment increased with increasing Ho concentration. These results suggest a mixture of high and low spin configuration due to the existence of two different crystallographic sites for cobalt in octahedral and trigonal prism. The values of $5.03 \mu_B$ and $5.37 \mu_B$ for the samples with $x = 0$ and $x = 0.01$, respectively are rather in good agreement with the mixed states of low spin $\text{Co}^{\text{II}} \sim 1 \mu_B$ and high spin $\text{Co}^{\text{III}} \sim 4 \mu_B$. For the samples with $x = 0.03$ and $x = 0.05$, the values μ_{eff} are much higher than $5 \mu_B$, suggesting a more complicated spin configuration of Co1 and Co2.

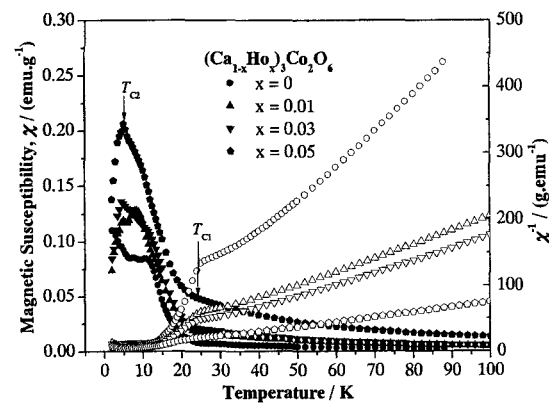


Fig.7 The magnetic susceptibility and inverse susceptibility of the samples measured upon heating at

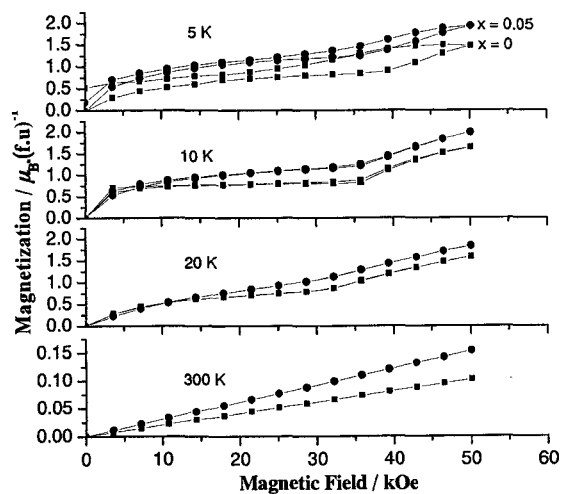


Fig.8 The magnetization curves measured at different temperatures of the non-doped sample.

From the thermal magnetization curves, the temperature ranges can be divided to be assigned to different magnetic states: $T > T_{C1}$, $T_{C2} < T < T_{C1}$ and $T < T_{C2}$. The whole picture of magnetic behavior can be observed from the magnetization as a function of

magnetic field measured at different temperatures (magnetization isotherms) through T_{C1} and T_{C2} . Fig. 8 shows the magnetization isotherms for the non-doped and a typical Ho-doped sample.

For $T \gg T_{C1}$, in agreement with the paramagnetic state of the compounds, the magnetization is proportional to the applied magnetic field and the curves are linear (for example at $T = 300$ K). For $T_{C2} < T < T_{C1}$, the intrachain ferromagnetic and interchain antiferromagnetic coupling are set up. For non-doped sample the interchain AF coupling is still too weak to force the ferrimagnetic installation. As the field increases, one can see an induced magnetization plateau (for example at $T = 10$ K). Then beyond a critical field about 3.5 T, magnetization jumps more or less abruptly to reach its saturation, indicating a field-induced transition. The magnetization plateau can not be observed for the Ho-doped samples due to the increase in the interchain AF interaction. For $T < T_{C2}$, the transitions remains abrupt but becomes irreversible as shown in the magnetization curves at 5 K.

As a summary, detailed magnetic phase diagrams of non-doped and the Ho-doped samples are proposed in Fig. 9. Four domains can be distinguished, corresponding to the paramagnetic (PM), partial antiferromagnetic (PAF), ferrimagnetic (FR) and ferromagnetic (FM) states. Below 5 K, the samples show irreversible properties due to complicated magnetic substructures at very low temperatures.

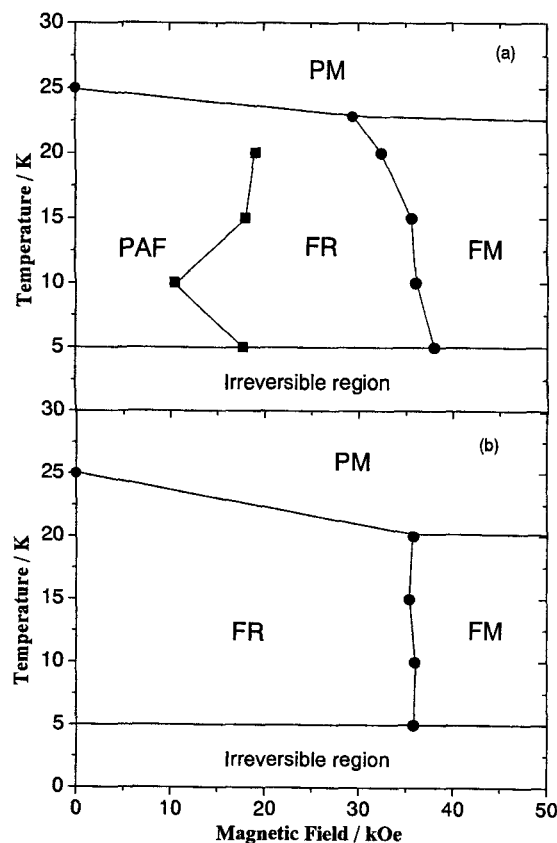


Fig.9 Magnetic phase diagrams, PM, PAF, FR and FM are for paramagnetic, a partial antiferromagnetic, ferrimagnetic and ferromagnetic states. (a) and (b) are for non-doped and the Ho-doped samples, respectively.

4. CONCLUSIONS

High temperature thermoelectric properties of the $(\text{Ca}_{1-x}\text{Ho}_x)_3\text{Co}_2\text{O}_6$ polycrystalline samples with $x = 0, 0.01, 0.03$ and 0.05 were investigated for the first time in detail from room temperature to 1300 K. At high temperatures, the figure-of-merit was improved remarkably by substitution of small amount of Ho^{3+} for Ca^{2+} due to the decrease in the thermal conductivity and the increase in the power factor.

Higher Ho concentration resulted in an increase in the AF interaction between Co-O chains and the enhanced effective moment of the samples. The magnetic structures to explain an enhancement of the effective magnetic moment for the samples with $x \geq 0.03$ need more evidences and further investigations.

References

- [1] S. Li, R. Funahashi, I. Matsubara, K. Ueno, S. Sodeoka, H. Yamada, *J. Mater. Sci. Lett.* **19**, 1339 (2000).
- [2] Y. Miyazaki, K. Kudo, M. Akoshima, Y. Ono, Y. Koike, T. Kajitani, *Jpn. J. Appl. Phys.* **39** L 531 (2000).
- [3] K. Fujita, T. Mochida, and K. Nakamura, *Jpn. J. Appl. Phys.* **40**, 4644 (2001).
- [4] R. Funahashi, I. Matsubara, H. Ikuta, T. Takeuchi, U. Mizutani, S. Sodeoka, *Jpn. J. Appl. Phys.* **39**, L 1127 (2000).
- [5] E. Woermann and A. Muan, *J. Inorg. Nucl. Chem.* **32**, 1457 (1970).
- [6] H. Kageyama, K. Yoshimura, K. Kosuge, H. Mitamura and T. Goto, *J. Phys. Soc. Jpn.* **66**, 1607-1610 (1997).
- [7] S. Aasland, H. Fjellvag and B. Hauback, *Solid State Commun.*, **101**, 187-192 (1997).
- [8] A. Maignan, C. Michel, A. C. Masset, C. Martin and B. Raveau, *Eur. Phys. J. B* **15**, 657-663 (2000).
- [9] K. Iwasaki, H. Yamane, S. Kubota, J. Takahashi and M. Shimada, *Journal of Alloys and Compounds*, 358, 210-215 (2003).
- [10] M. Hernando, B. Matinez, V. Laukhin, V. Fontcuberta, M. Parras, *J. Magn. Magn. Mat.*, **242**, 757-759 (2002).
- [11] M. Mikami, R. Funahashi, M. Yoshimura, Y. Mori and T. Sasaki, *J. Appl. Phys.*, **94**, 6579-6582 (2003).
- [12] Ji-Woong Moon, Yoshitake Masuda, Won-Seon Seo, Kunihito Koumoto, *Materials Science and Engineering*, B85, 70-75 (2001).

(Received December 11, 2005; Accepted March 31, 2006)